

THE MICROSTRUCTURE AND STRENGTH PROPERTIES OF MA957 NANOSTRUCTURED FERRITIC ALLOY JOINTS PRODUCED BY FRICTION STIR AND ELECTRO-SPARK DEPOSITION WELDING—P. Miao, G. R. Odette (University of California, Santa Barbara), J. Gould, J. Bernath (Edison Welding Institute), R. Miller (DDL-OMNI), M. Alinger (University of California, Santa Barbara, University of California, Berkeley) and C. Zanis (DDL-OMNI)

OBJECTIVE

This work is to investigate joining methods and their effects on microstructures and mechanical properties of nanostructured ferrite alloys.

SUMMARY

The nanostructured ferritic alloy (NFA) MA957 was joined by friction stir welding (FSW) and electro-sparked deposition (ESD) welding. Transmission electron microscopy (TEM) and small angle neutron scatter (SANS) characterization studies showed a uniform fine-scale equiaxed ferrite structure with a high density of dislocations and only slightly coarsened nm-scale particles in the joint region of the FSW weld compared to the base metal. Microhardness and tensile measurements on the FSW showed a modest reduction in the strength of the joint compared to the as-processed MA957. In contrast, the ESD welds contained considerable porosity and the nm-scale particles dissolved or coarsened significantly, resulting in a larger degradation of the joint region strength. Thus FSW is a promising method for joining NFAs.

PROGRESS AND STATUS

Introduction

Nanostructured Fe-14Cr-W-Ti-Y₂O₃ dispersion strengthened ferritic alloys (NFAs) have outstanding low temperature tensile (> 1 GPa) and high temperature creep strengths [1-3] and also offer a potential for mitigating radiation damage, including the effects of high helium levels [4, 5] in fusion reactor environments. The excellent properties of NFAs primarily derive from a very high density of Y-Ti-O nm-scale precipitate phases that form when mechanically alloyed powders (pre-alloyed Fe-14Cr-W-Ti plus Y₂O₃) by milling are consolidated by hot isostatic pressing (HIPing) or extrusion [5-8]. These phases include small solute clusters rich in Y-Ti and O and slightly larger Ti₂Y₂O₇ pyrochlore oxides. Henceforth, we will refer to these features as nm-scale particles (NSP) encompassing a size range up to ≈ 8 nm. Thus, a critical issue is producing and maintaining the NSP through all stages processing and fabrication, as well as in high temperature service in irradiation environments.

Thus a major challenge to the use of NFAs is joining. Conventional fusion welding methods are generally not useful, since the NSP would be expected to dissolve during typical melting-solidification processes. Joining processes, that either avoid melting completely, or that involve very rapid melting and re-solidification, may preserve the NSP. In this work we explore two such possible joining methods. FSW is a solid-state joining process that involves mechanical mixing of base metals under severe deformation conditions [9, 10]. The material in and near a FSW joint experiences a moderately high temperature cycle, with peak temperatures up to ≈1300 to 1400°C, but there is no melting. Thus, in principle, FSW may or may not severely damage the NSP. Further, dynamic recrystallization during FSW refines the grains in the stir zone, and further severe deformation induces a high dislocation density [11, 12]. Thus, fine scale FSW microstructures may provide an optimal balance of mechanical properties. ESD welding uses a rapid discharge power source to supply short-duration current pulses to a moving electrode in contact with a substrate [13]. The pulses produce extremely rapid heating, leading to melt droplet formation and deposition in the weld zone as relatively thin splats that cool at very high rates. Thus, in principle, the rapid ESD temperature cycle might allow some of the NSP to survive in the joint region.

Experimental

A commercial MA957 alloy bar of 25mm (diameter) \times 100mm (length) with a nominal composition of Fe-14wt% Cr, 0.9% Ti, 0.3% Mo, and 0.25% Y_2O_3 was sectioned into $100 \times 17 \times 2 \text{ mm}^3$ and $10 \times 17 \times 2 \text{ mm}^3$ slabs for FSW and ESD welding, respectively. FSW butt-welding in the long dimension direction was produced at a tool spindle speed of 130 to 160 rpm and travel speed of 150 – 200 mm/min [10]. Other details of the FSW method and tooling are proprietary. The ESD but-welding was performed with an electrode ground from the MA957 using an Advanced Surfaces and Processes (ASAP) system at a pulse rate of 400 Hz and voltage of 150 V. The butted base metal sections were ground to a \approx half thickness radius and then filled by the ESD deposit, one side at a time.

The nano-microstructures of the MA957 weld and base metals were characterized by TEM (JEOL2010HR), SANS (NG1 at the National Institute of Standards and Technology) and optical microscopy. Standard 3 mm TEM discs, either centered in the weld region or taken from the base metal, were ground to a thickness of $\sim 0.15 \text{ mm}$ and then thinned to electron transparency in a TENUPO twin-jet electro-polisher with $H_2SO_4 + 80\%CH_3OH$ at room temperature. TEM images for the measurement of the NSP and larger oxide particles were taken in the same foil orientation (near [011]) for the MA957 weld and base metals. Details of the experiment, data reduction and analysis for SANS are given elsewhere [14].

The room temperature strength of the FSW and ESD-welded MA957 were evaluated both by microhardness traverses across the weld and tensile tests using subsized flat dogbone specimens with a reduced gauge section in the weld and heat-affected zone transverse to the weld axis. The corresponding tensile tests carried out on the base metal were for the same orientation.

Results and Discussion

As seen in Figure 1a, the MA957 base metal has typical fine scale elongated ferrite grains along the extrusion direction. In contrast, as seen in Figure 1b, the severe plastic deformation during FSW produces a uniform distribution of fine scale equiaxed grains, containing a significant density of dislocations. The optical macro and micrographs in Figure 2 show that after the ESD welding process produces a layered structure, composed of large number of droplet-scale deposits (Figure 2a) along with considerable porosity (Figure 2b). Such structures are typical of ESD depositions carried out in air, and clearly do not represent an acceptable joint product. Note, however, the process could be modified to minimize the porosity. Thus the major issue of concern here for the ESD welds is the fate of the NSP.

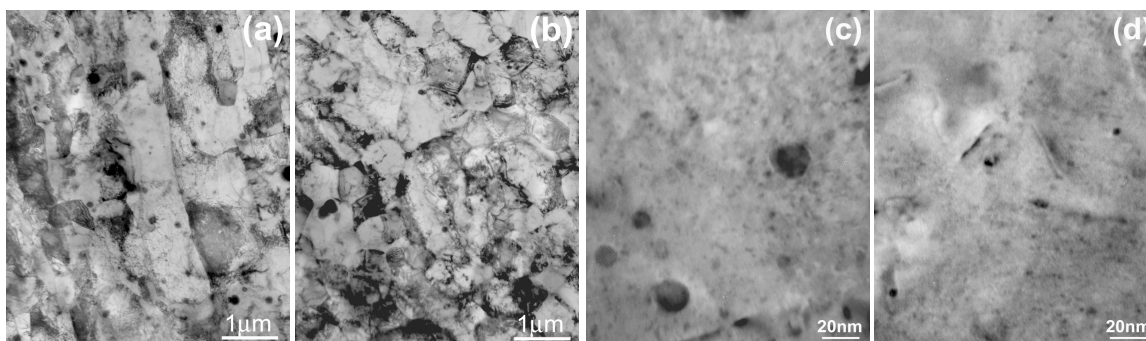


Figure 1. TEM image of the grain and dislocation microstructure in the MA957 (a) base metal and (b) FSW and the NSP and larger oxide particles in (c) base metal and (d) FSW.

As seen in the TEM micrographs in Figures 1c and d, there is a high density of NSP in both the base (Figure 1c) and FSW weld (Figure 1d) metals. Based on convergent beam estimates of the foil thickness, the particle size and volume fraction distributions are shown in Figures 3a and b and the corresponding

NSP parameter averages are shown in Table 1. Note rather large particles, with diameters greater than about 8 nm, are included in these assessments, and represent what is considered to be a second population of oxide phases that contribute significantly to the overall volume fraction estimated by TEM.

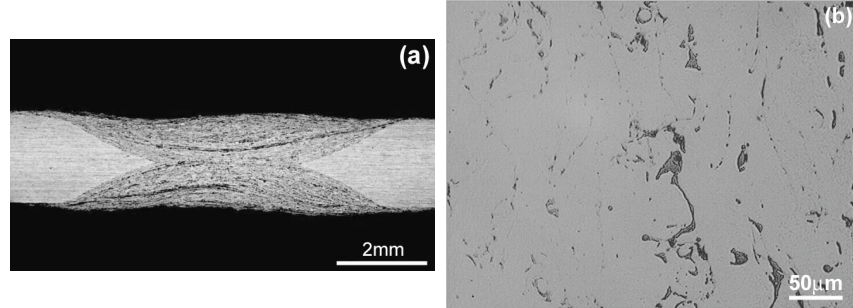


Figure 2. (a) Macrograph and (b) micrograph (unetched) of the MA957 ESD weld.

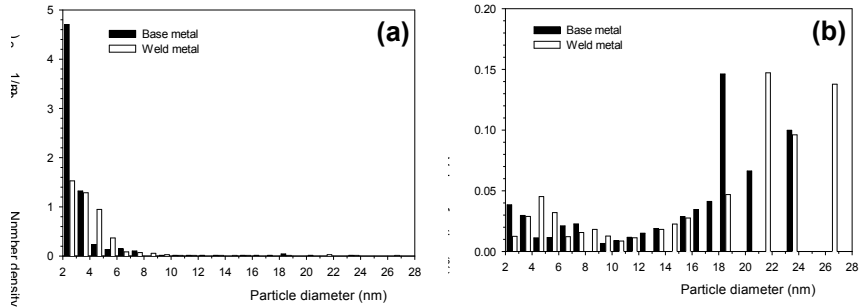


Figure 3. (a) The number density and (b) the volume fraction of the NSP and larger oxide particles in the MA957 FSW and base metal found in the TEM studies.

Table 1. The average NSP and larger oxide particle parameters found in the TEM studies and NSP parameters measured by the SANS in the MA957 FSW, ESD and base metal

NSP and Larger Oxide Parameters		Base metal	FSW	ESD
Average diameter (nm)	TEM	3.4	4.1	
	SANS	2.4	2.5	4.7
Number density ($\times 10^{23}$, $1/m^3$)	TEM	0.68	0.45	
	SANS	8.5	3.5	0.25
Volume fraction (%)	TEM	0.61	0.69	
	SANS	0.6	0.25	0.12

The TEM on the FSW shows only a slight coarsening of the NSP, with a nominal increase in the particle diameter from ≈ 3.4 to 4.1 nm and a reduction in number density from ≈ 0.68 to $0.45 \times 10^{23}/m^3$. The volume fraction is approximately constant of $\approx 0.67\%$ (FSW) versus 0.6% (base metal). However, there are two important caveats. First, the smallest NSP cannot be imaged in TEM. Second the features observed in TEM may include some surface deposit artifacts. Both of these limitations indicate the need for the use of other techniques.

SANS characterization of both the FSW and ESD joints was carried out on the NG1 instrument at NIST. Because of the small size and somewhat irregular shape of the weld specimens, it was not possible to

experimentally establish the magnetic to nuclear scattering ratio (M/N) in this case. However, the relative shapes and positions of the SANS curves at 45° to the direction of the magnetic field, shown in Figure 4, can be qualitatively interpreted to show that FSW decreases the number density and volume fraction and spreads the size distribution of NSP. The ESD process has a larger effect, leading to a greater increase in the size and a large reduction in the number density and volume fraction of the NSP. The absolute magnitudes of the scattering curves can be estimated assuming a typical $M/N = 1$ for MA957. Corresponding fits to these cross sections, assuming the particles are non-magnetic, can be used to derive the NSP parameters that are summarized in Table 1.

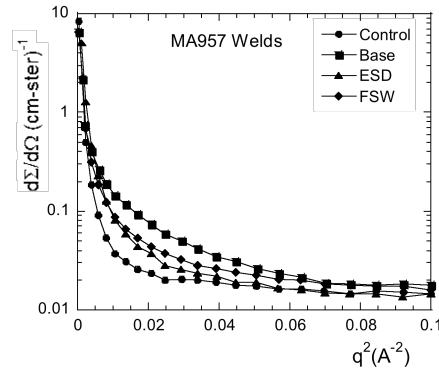


Figure 4. SANS cross section curves at a 45° angle to the direction of the magnetic field.

Clearly the SANS shows the presence of smaller and more numerous NSP compared to TEM. This is expected since: a) the SANS is optimized to detect small NSP features while it is blind to the larger features; and b) TEM does not see the smallest and most numerous NSP.

Because of their limitations, neither the SANS nor TEM quantitative results should be taken too literally. However, they are broadly consistent with each other, and clearly show that while FSW reduces the number and volume fraction of NSP, the overall effects are relatively modest. In contrast the ESD welding process has a much larger effect on the NSP, consistent with a larger reduction in their hardening contribution, by estimated factors of at least 2 to 4, depending on assumptions about changes in the particle strength factors as obstacles to dislocation glide.

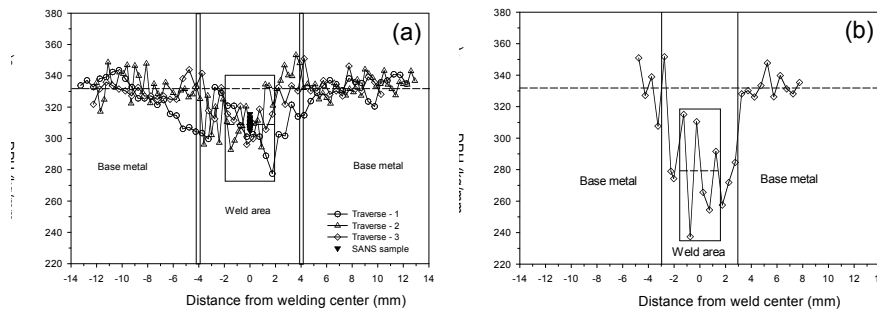


Figure 5. Microhardness profile across the welds of (a) FSW- and (b) ESD-welded MA957.

Vicker's diamond pyramid hardness (DPH) traverses at 500g load across the FSW and ESD welds are shown in Figure 5. Figure 5a for the FSW also includes measurements on a SANS specimen on the weld axis. The strength decreases from the edge of the weld and is a minimum near the center. The average DPH value in the central weld region of the FSW-welded MA957 for various indent sequences ranged from $309 \pm 10 \text{ kg/mm}^2$ or about 7% lower than for the base metal value of $332 \pm 10 \text{ kg/mm}^2$. In contrast, the

average DPH ($279 \pm 31 \text{ kg/mm}^2$) in the central weld region of the ESD-weld shown in Figure 5b is $\approx 16\%$ lower compared the base metal.

As shown in Table 2, the ultimate tensile strength UTS was decreased by $\approx 9\%$ in the FSW and by $\approx 37\%$ in the ESD weld. Thus tensile results for the FSW are consistent with the decrease in hardness in the weakest part stir zone. The larger decrease in the tensile strength of the ESD weld, compared to the hardness drop, is probably due to the presence of porosity in this case.

Table 2. UTS of base and weld metal in the FSW- and ESD-welded MA957

Property	Base metal	FSW	ESD
UTS (MPa)	1035 ± 3	942	656^a

^aOnly one specimen was tested.

Discussion

With regard to the key question about the fate of the NSP, the SANS results of this study suggest that FSW produces a larger degradation of the smallest features, but even in this case it is on the order of a 50% reduction in the number density and volume fraction. Somewhat larger features are only slightly coarsened. This behavior may be due to a combination of the transient high temperatures during FSW, and very severe deformation that results in mechanical dissolution of the small particles by dislocation cutting processes. This conclusion is consistent with the previous observation that small NSP are not strong dislocation Orowan-type barriers. Note, such mechanical cutting may also play a role in the initial mechanical alloying process. The FSW also produces beneficial changes in the microstructure, by refining the grains and making them equiaxed, as well as increasing the dislocation density. The net result is a minimal decrease in the strength of the FSW joint ($<10\%$). In contrast to the FSW case, the ESD joining process appears to be far less promising. In spite of the rapid sequence of melting and solidification the NSP are severely degraded.

Summary and Conclusions

The FSW produced an attractive high strength joint of MA957 with a uniform fine-scale and equiaxed ferrite structure as well as a significant density of dislocations in the severely plastically deformed joint stir region. The NSP were only slightly degraded during welding in this case. FSW decreased the alloy hardness and ultimate tensile strength by less than 10% compared to the base metal. The ESD MA957 welds contained porosity and the NSP were severely degraded during the melting-resolidification sequence. These microstructural changes resulted in a significant degradation of mechanical properties from $\approx 16\%$ (hardness) to $\approx 37\%$ (UTS) compared to the MA957 base metal. Hence, ESD welding does not appear to be a promising method for joining NFA.

References

- [1] M. J. Alinger, G. R. Odette, and G. E. Lucas, *J. Nucl. Mater.* 307-311 (2002) 484.
- [2] R. L. Klueh, J. P. Shingledecker, R. W. Swindeman, and D. T. Hoelzer, *J. Nucl. Mater.* 341 (2005) 103.
- [3] R. L. Klueh, P. J. Maziasz, I. S. Kim, L. Heatherly, D. T. Hoelzer, N. Hashimoto, E. A. Kenik, and K. Miyahara, *J. Nucl. Mater.* 307-311 (2002) 773.
- [4] T. Yamamoto et al., *Journal of Nuclear Materials* (to be published).
- [5] M. J. Alinger, G. R. Odette, and D. T. Hoelzer, *J. Nucl. Mater.* 329-333 (2004) 382.
- [6] M. K. Miller, D. T. Hoelzer, E. A. Kenik, and K. F. Russel, *J. Nucl. Mater.* 329-333 (2004) 338.
- [7] S. Ukai and M. Fujiwara, *J. Nucl. Mater.* 307-311 (2002) 749.
- [8] M. Klimenkov, R. Lindau, and A. Möslang, *J. Crystal Growth* 249 (2003) 381.
- [9] W. M. Thomas and E. D. Nicholas, *Materials & Design* 18 (1997) 269.
- [10] J. Bernath and J. Gould, Report on Development of Candidate Joining Technology for MA957 Sheet, March 2005, Edison Welding Institute, Columbus, Ohio, USA.

- [11] Y. S. Sato, T. W. Nelson, C. J. Sterling, R. J. Steel, and C.-O. Pettersson, *Mater. Sci. Eng. A397* (2005) 376.
- [12] K. V. Jata, K. K. Sankaran, and J. J. Ruschau, *Metall. Mater. Trans. 31A* (2000) 2181.
- [13] G. L. Sheldon and R. N. Johnson, *Electro-spark deposition—a technique for producing wear resistant coatings*, Ed., K. C. Ludema, *Wear of Materials*, ASME, New York, 1985.
- [14] M. J. Alinger, Ph.D. dissertation, University of California, Santa Barbara, 2004.